Precipitation Processes within an Alberta Supercell Hailstorm

TERRENCE W. KRAUSS[1] AND JOHN D. MARWITZ

Department of Atmospheric Science, University of Wyoming, Laramie, WY 82071

(Manuscript received 20 January 1983, in final form 16 November 1983)

ABSTRACT

An investigation was made into the precipitation processes operating within an Alberta supercell hailstorm which occurred on 22 July 1979. The main research tools employed in the study were an instrumented aircraft and an S-band meteorological radar.

Five cloud penetrations were conducted in and around the bounded weak-echo region associated with the main updraft of the storm during a 40 min period while the storm was producing 2–5 cm diam hail at the surface. The main updraft consisted of a relatively smooth, steady flow with adiabatic temperature. The main updraft acted as an obstacle to the mid-level environmental flow and caused the winds to split and accelerate around the southern side. Several smaller turbulent updrafts associated with time-dependent, fine-scale convective cells (feeder clouds) existed adjacent to the main updraft and appeared to be superimposed onto the quasi-steady, broader-scale dynamically forced circulation of the main storm. Graupel particles which originated within the feeder clouds were transported by the mid-level winds into and across the weak-echo region.

This study provides evidence that feeder clouds are also found within storms classed as supercells and that they provide a viable source of hailstone embryos and present a vital link among hail formation processes within a broader-scale continuum of hailstorm structures.

1. Introduction

The hailstorm poses a serious threat to agriculture in the province of Alberta. As a result, hail suppression has remained at the forefront of atmospheric research for the last several decades. Nevertheless, our present understanding of hail formation processes is incomplete. In Alberta, radar reflectivity data (Barge and Bergwall, 1976) and numerical hail growth models (English, 1973) have been used to develop conceptual models of hail formation processes. However, direct observations of the microphysical composition, thermodynamic structure, and kinematic features outside of the storm's precipitation filled volume are lacking.

Beginning with the Thunderstorm Project (Byers and Braham, 1949), a growing body of quantitative knowledge concerning thunderstorms has evolved. Marwitz (1972a,b,c) proposed several categories of hailstorms as supercells, multicells, squall line, and severely sheared storms based upon echo structures which seemed to be functions of environmental wind shear and convective instability. Browning (1977) modified this empirical classification as far as the hail producing mechanism was concerned to include only the ordinary cell versus the supercell. A relatively small number of supercell thunderstorms which are prolific producers of severe weather, are characterized by a radar identifiable structure (Browning, 1965a,b) with the updraft and downdraft coexisting for periods which are long compared to the time taken for air to pass through them.

The principal objective of this research was to ascertain the microphysical characteristics and determine the dominant process of hydrometeor development within the convective region located upwind (with respect to the mid-level winds) of a mature Alberta hailstorm. This region has been called the "new growth zone." The main research tools employed were the University of Wyoming's instrumented Queen-Air aircraft (N10UW) and the Alberta Research Council's S-band meteorological radar. The aircraft data system has been described by Cooper and Saunders (1980) and the radar system has been described by (Humphries and Barge, 1979).

This paper summarizes the precipitation processes in the new growth zone of the Acme storm which occurred on 22 July 1979. The storm is classified as a supercell since a persistent echo-free vault (Browning and Ludlam, 1962; Browning and Donaldson, 1963) or bounded weak-echo region (BWER), as referred to by Chisholm (1970), existed for over 1.5 h on the storm's right-front flank. Five storm penetrations were made during a 40 min period while the storm was producing 2–5 cm diam hail at the surface. The aircraft microphysical and dynamic measurements are presented relative to the radar PPI and vertical cross section data. The main significance of this research is that it provides direct observational evidence to support

[1] Present affiliation: Alberta Research Council, Edmonton, Alberta, Canada.

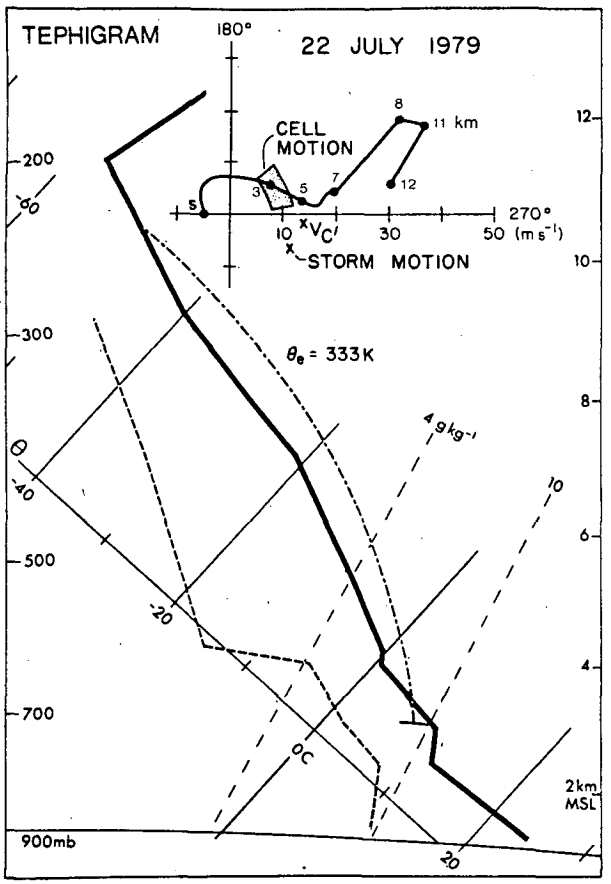

FIG. 1. The environmental sounding taken at 1800 MDT at Calgary. The hodograph shows the storm motion (×) and the × labeled $V_{c'}$ refers to the motion of two cells on the extreme southern edge of the storm. The shaded envelope represents the general cell motion.

the hypothesis of Barge and Bergwall (1976) that time-dependent, fine-scale convective cells (feeder clouds[2]) are found within supercell storms and that they provide a viable source of hailstone embryos and present a vital link among hail formation processes within a broader-scale continuum of hailstorm structures.

2. Character of the environment

The representative environmental sounding and hodograph for the storm are shown in Fig. 1. The estimated conditions at cloud base (temperature 6°C, mixing ratio 8.2 g kg^{-1}) are indicated. The cloud base temperature θ was ~1.5 K colder than the environment, implying that the updraft at cloud base contained negative thermal buoyancy, a common observation in updrafts beneath Colorado thunderstorms (Marwitz, 1972a; Foote and Fankhauser, 1973).

The environmental wind shear computed from cloud base to the top of the positive energy layer was $\sim 4.0 \times 10^{-3}$ s^{-1}. The subcloud environmental winds were 5–8 m s^{-1} and veered about 130° within the subcloud layer. The hodograph bears a striking resemblance to the typical hodograph for supercell storms, as discussed by Marwitz (1972a). The storm motion (from 295° at ~12 m s^{-1}) is indicated on the hodograph. Cells (identified by fine-scale radar reflectivity maxima) tracked roughly with the 4 km winds, although two cells, similar to the persistent cores within the severe Alberta hailstorm studied by Marwitz and Berry (1971), tracked significantly to the right of the mean tropospheric winds. The motion of these cells is indicated on the hodograph by the vector $V_{c'}$.

3. General description of the storm

The locations of the hailfall reports at the surface and the flight track of N10UW are shown in Fig. 2. The hailfall lasted from 1950 to 2230.[3] Golfball (3.3–5.2 cm diam) size hail fell at 2050, and walnut (2.1–3.2 cm diam) size hail fell at five locations between 2100 and 2130. The reported hailstone shapes and surface textures varied greatly: round, conical, and flat stones fell, and their surface textures varied from smooth to raspberry-like and knobby. Some reports indicated that 90% of the hailstones were soft and slushy, but an equal number of reports indicated that all were hard. The hailstone characteristics were not apparently related to size, location or time and a variety of particle trajectories must have coexisted within the storm. Two hail samples were collected for hail embryo analysis. The maximum hail sizes were 18 and 22 mm and only graupel embryos were found.

4. Detailed three-dimensional radar structure

The 2.2° elevation PPIs at 2051 and 2127 are shown in Fig. 3. The BWER is clearly evident as are many cells coexisting in time. The radar operated at a 0–20° elevation spiral scan and PPIs at each degree of elevation were recorded on magnetic tape at 3 min intervals. This permitted the tracking of some of the cells. The tracks of 16 cells with respect to the ground are also shown in Fig. 3. The cell tracks relative to the storm motion were predominantly northerly. The WER influenced the motion of cells near it. Cells usually deviated around the WER either to the west or to the east, while some cells ascended rapidly and lost their discrete identity above the WER.

The 2.2° elevation PPI at 2103:42 is shown in Fig. 4. The line AB is drawn parallel to the propagation vector, intersecting the high reflectivity core and ex-

[2] The definition of the term "feeder cloud" in this study is the same as that specified by Heymsfield *et al.* (1980). A feeder cloud can have a strong updraft and is capable of growing hail. Also, particles can be advected from a feeder cloud into the main updraft region of a storm.

[3] All times local Mountain Daylight.

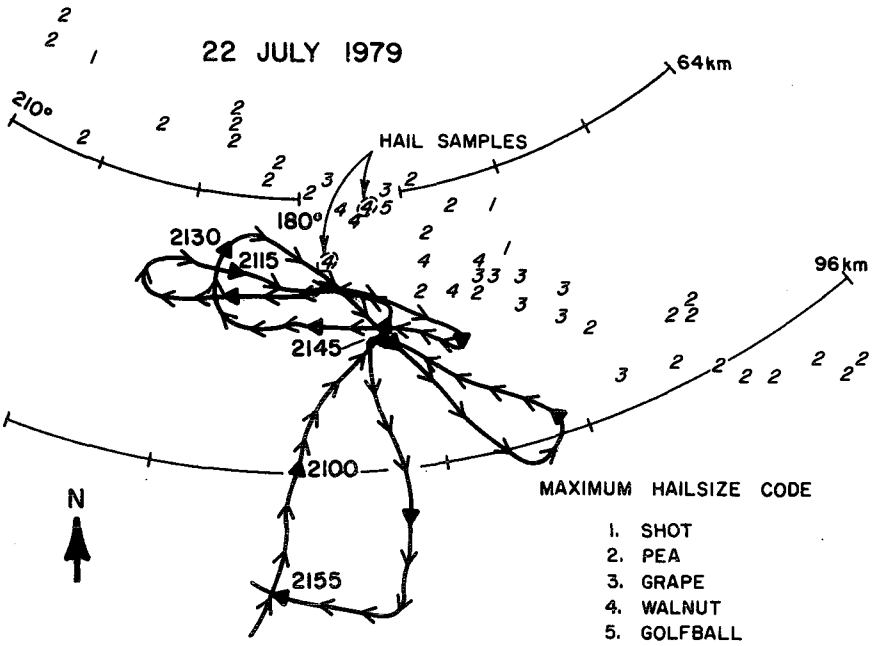

FIG. 2. Flight track of N10UW from 2055 to 2155. Arrows are located at 1 min intervals with a solid arrow every 5 min. The locations of the hail reports and two hail samples are shown.

tending southeastward across the WER. The propagation vector is the difference between the cell motions and the storm motion. The time sequence of radar vertical cross sections along the storm propagation vector from 2103 to 2115 is shown in Fig. 5. Some of the cells are labeled. The cross sections along the propagation vector intersect several cells, each at a different stage in their evolution. The cells toward the right (northwest) were in their dissipating stage and accounted for the hailfall at the surface. The cells toward

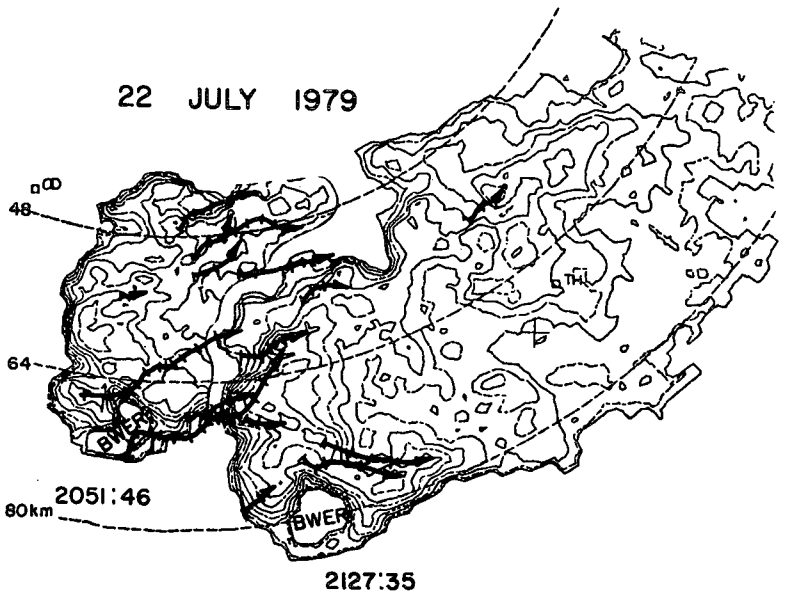

FIG. 3. The locations of the Acme storm echo at 2051 and 2127. The PPI elevation angle is 2.2°. Reflectivity contours are at 5 dB(Z) intervals starting at 20 dB(Z). The tracks of 16 cells with respect to the ground are shown. Tick marks are at 3 min intervals.

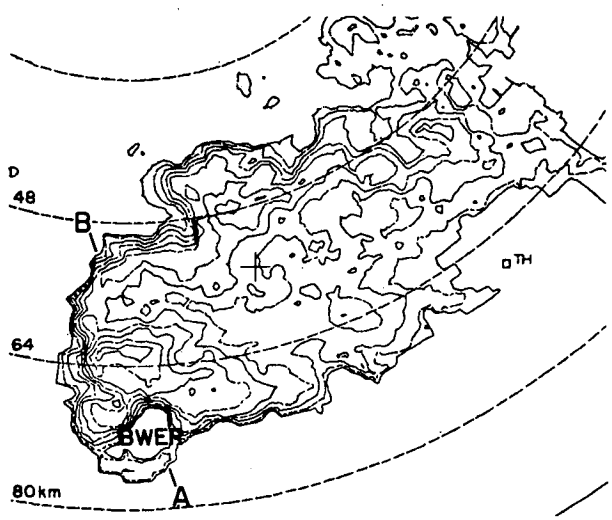

FIG. 4. The 2.2° elevation PPI at 2103. Line AB represents the storm propagation vector intersecting the high reflectivity core and extending across the WER toward the new growth zone.

the left (southeast) were in their developing stages and represented the new growth which caused the storm as a whole to deviate (propagate) to the right of the mean tropospheric winds. The location of N10UW during the first and second penetrations is shown in the 2109 and 2115 panels. The vertical cross sections illustrate the quasi-steady nature of the main storm updraft and associated BWER. Cells, approximately 2–5 km in horizontal extent, which appeared to originate on the upwind edge of the BWER, traveled over and around the main updraft and exhibited rapid increases in reflectivity.

5. Storm structure from aircraft penetrations

The time segments and some of the meteorological data corresponding to the cloud penetrations are listed in Table 1. The clouds had continental cloud droplet size distributions. Each penetration was along the southwestern flank of the storm, near and within the WER. The southwestern flank of the storm continually contained several vigorous feeder clouds which did not produce radar echoes [the minimum detectable signal at the range of the storm is approximately 20 dB(Z)] prior to merging with the main storm mass. A photograph of the new growth zone taken slightly before the second cloud penetration is shown in Fig. 6. The setting sun highlighted some of the developing feeder cloud tops in the vicinity.

The storm was seeded at cloud base with 15 end-burning 150 g AgI pyrotechnics between 2100 and 2145. However, the seeding occurred 10–20 km northwest (downwind) of the BWER. The measurements by N10UW are not thought to have been affected by the cloud seeding since the cloud regions which were penetrated were upwind and considerably removed in space and time.

The track for penetration 1 and the 2.2° elevation PPI at 2109 are shown in Fig. 7. The aircraft passed immediately south and slightly below the echo forming

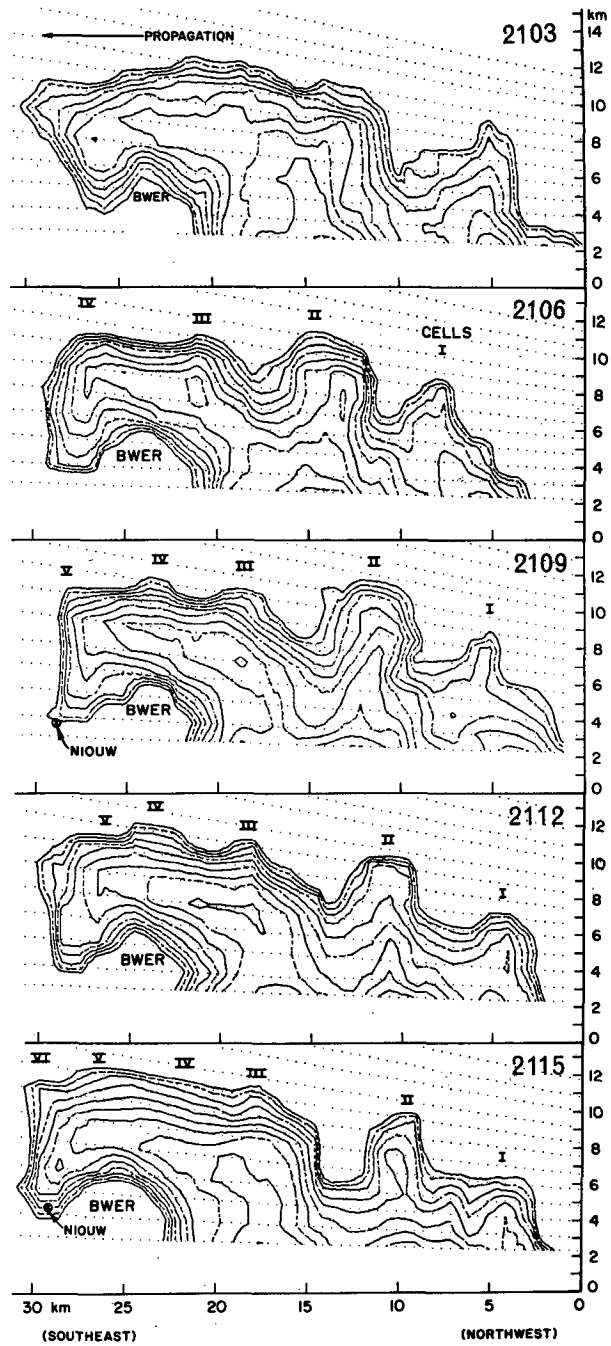

FIG. 5. The sequence of radar vertical cross sections along the storm propagation vector (line AB in Fig. 4) from 2103 to 2115. Reflectivity contours are at 5 dB(Z) intervals starting at 20 dB(Z). Several cells are labeled and the location of N10UW during the first two penetrations is shown.

TABLE 1. Summary of cloud penetration data. Values are maximum 1 s values except where an overbar implies a mean value for the penetration. The penetration of radar echo > 20 db(Z) is also indicated.

Penetration	Time (MDT)	Length (km)	$\overline{\text{Altitude}}$ (km)	$\overline{\text{Temperature}}$ (°C)	θ_E (K)	JW LWC (g m^{-3})	ASSP CONC (cm^{-3})	ASSP $\bar{D}$ (μm)	Updraft (m s^{-1})	Downdraft (m s^{-1})	$\bar{\epsilon}$ (cm^2 s^{-3})	Ice Concentration Total (L^{-1})	Ice Concentration $D > 200$ μm (L^{-1})	Echo
1.	2106:20–2111:00	21.0	3.9	−0.2	333.5	1.1	missing		10	4	22.	<1	<1	N
2.	2115:15–2117:30	10.1	5.0	−7.1	333.5	1.3	849	16.1	18	4	65.	33	12	Y
3.	2123:10–2126:10	13.5	4.9	−8.7	331.9	1.2	612	13.4	12	4	114.	52	38	Y
4.	2131:20–2135:40	19.5	4.7	−6.6	332.4	1.2	786	14.8	12	8	114.	92	31	Y
5.	2142:20–2145:05	12.4	4.3	−3.3	332.0	1.1	739	13.9	21	5	35.	162	25	Y

the BWER (see also Fig. 5). Vectors representing 30 s average winds relative to the storm motion are plotted along the track. The wind vector direction is toward the flight track. Strong storm inflow (15–20 m s^{-1}) was detected as N10UW approached the storm from the southeast. A wind shift occurred between 2110 and 2111 as the flow appeared to separate around the storm near this apparent stagnation point. Two distinct updrafts of 10 m s^{-1}, each approximately 1 km wide, were observed at 2110:20 and 2110:45. These two updrafts on the southwest edge of the BWER are thought to have been associated with merging feeder clouds.

Precipitation sized particles were not observed during the penetration; therefore, it is doubtful that the 20 dB(Z) echo immediately above the flight altitude (Fig. 5) formed as a result of particles which rose in a single ascent from cloud base. The echo was more likely due to particles descending from above.

The track for penetration 2 and the 2.2° elevation PPI at 2115 are shown in Fig. 8. A peak 5 s mean wind velocity of 44 m s^{-1} was measured on the southeast corner of the BWER. The environmental winds at 5 km were 14 m s^{-1} (Fig. 1); therefore, the observed wind speed exceeded the environmental wind speed in this region by a factor of 3. The BWER was acting as an obstacle to the environmental flow and the accelerated flow can explain the rapid cell motion which was observed within the southern limb of the BWER.

Some of the measured parameters for cloud penetration 2 are shown in Fig. 9. A peak updraft of 18 m s^{-1} with adiabatic equivalent potential temperature (θ_e) was measured within a cell on the western side of the BWER. The echo was penetrated near 2116:10 and was associated with turbulent updrafts of 2–8 m s^{-1}. A second peak updraft of 13 m s^{-1} occurred at 2116:35 near the BWER. The two maximum updrafts were found to have light turbulence. The nearly constant

FIG. 6. Photograph taken from N10UW at 2114 looking southeast toward the new growth zone feeder clouds.

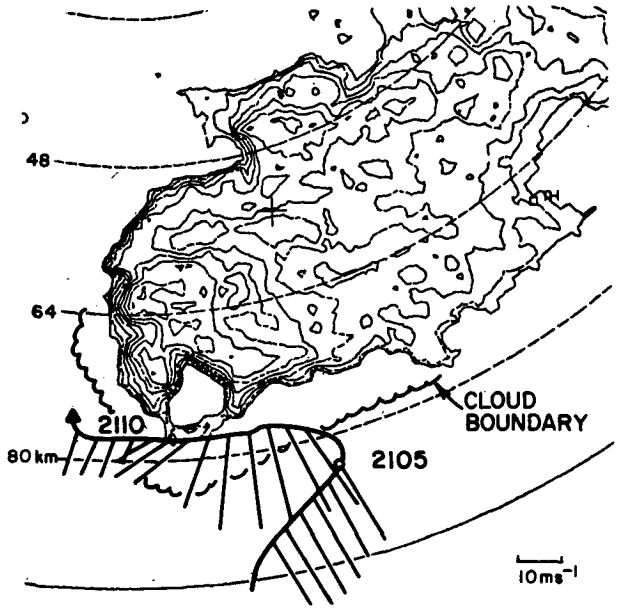

FIG. 7. The 2.2° elevation PPI at 2109. Reflectivity contours are at 5 dB(Z) intervals starting at 20 dB(Z). The aircraft track for penetration 1 is shown with wind vectors plotted relative to the storm. The wind vector direction is toward the track.

θ_e trace within both updrafts indicates that they were adiabatic.

The liquid water concentration measurements were questionable on this day. The Johnson-Williams (JW) hot-wire device measurements were typically half the adiabatic value. A subsequent wind-tunnel calibration of the instrument revealed that the JW was unable to measure water concentrations much above 1.0 g m^{-3}. The JW trace appeared to be clipped near 1.2 g m^{-3}. The Axially Scattering Spectrometer Probe (ASSP) was operating at below normal laser power levels and this

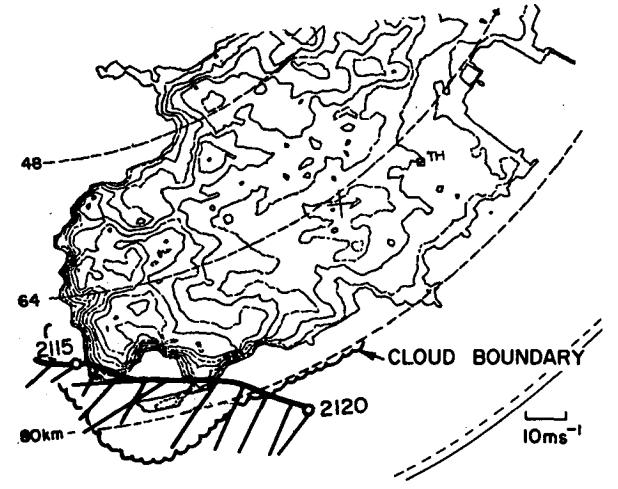

FIG. 8. As in Fig. 7, except the PPI is at 2115 and the aircraft track is for penetration 2.

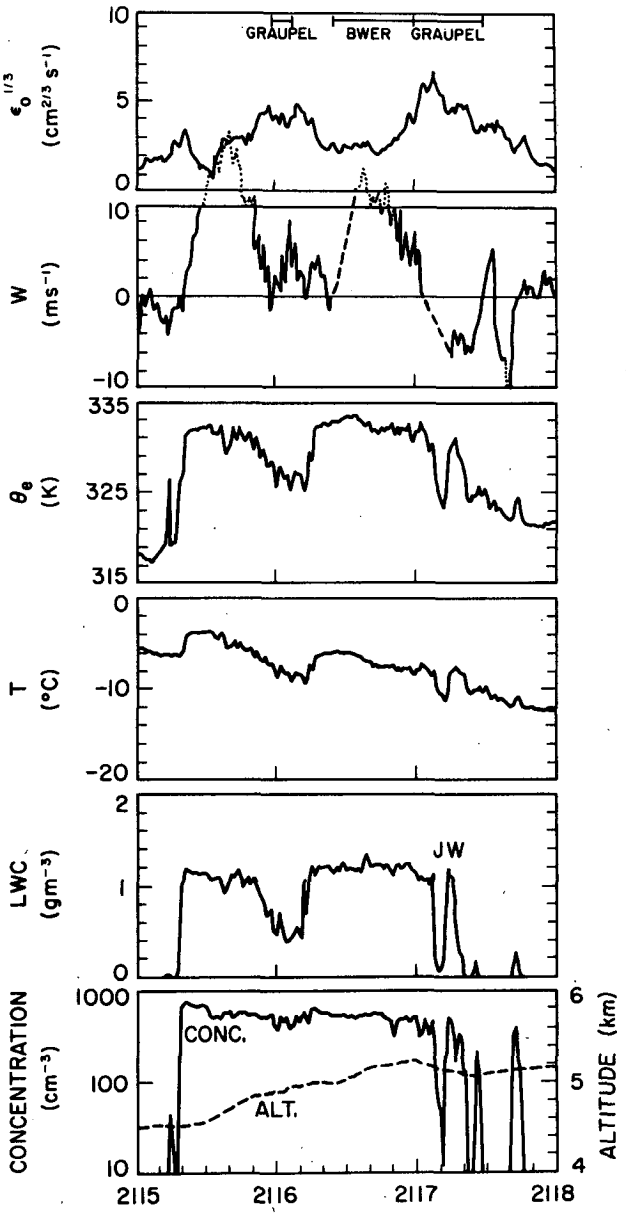

FIG. 9. Analog traces of indicated eddy dissipation rate, vertical wind, equivalent potential temperature, temperature, JW liquid water content, cloud droplet concentration, and altitude for penetration 2 of the Acme storm. The locations of the bounded weak-echo region (BWER) and the observation of graupel particles is indicated.

resulted in reduced counting and sizing of the cloud droplets. Considering the near adiabatic temperatures, one can assume that the liquid water contents should have also been near adiabatic (3 g m^{-3}).

All of the cloud particle images recorded by the Particle Measuring Systems 2D-C optical array spectrometer probe while penetrating the radar echo (2116:02 to 2116:16) are shown in Fig. 10. The particle size distribution is shown in Fig. 11. A nearly uniform distribution of graupel particles from 100 to 2000 μm in diameter, with a lack of small ice particles at high

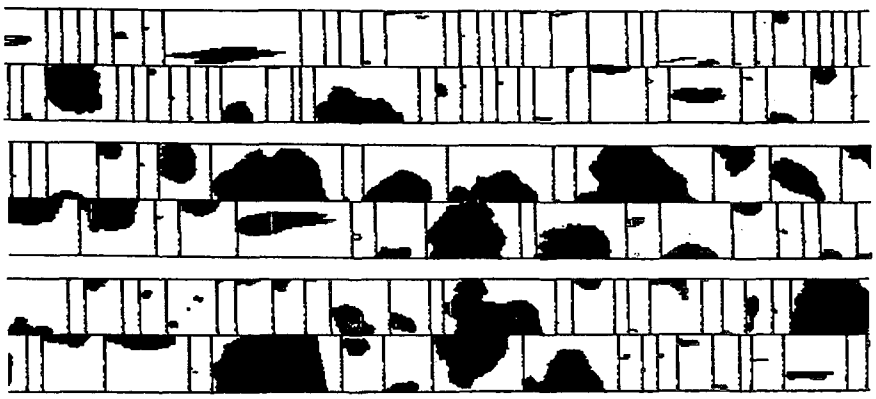

FIG. 10. Graupel images from an optical array spectrometer probe recorded from 2116:02 to 2116:16 as N10UW penetrated the echo on the western edge of the BWER. The distance between horizontal lines is 800 μm and the vertical lines between images are coded time bars.

concentrations, is indicative of size sorting within the updrafts. The 1–2 mm graupel with concentration of $\sim$0.15 L^{-1} can account for the 25 to 30 dB(Z) reflectivity. The graupel particles were still growing since they were located in a region of 2–5 m s^{-1} updraft with liquid water content > 0.4 g m^{-3}. The cloud particle data are consistent with the hypothesis that the echo was due to particles which descended into the WER.

The aircraft track for penetration 5 and the 2.2° elevation PPI at 2142:30 are shown in Fig. 12. Although the S-band radar PPI indicated a complete BWER, the echo on the southeast corner of the BWER (altitude 4.8 km) was slightly above the altitude of N10UW at 2143:00 (4.1 km). Fig. 13 shows some of the measured parameters during the penetration. The edge of the main updraft was encountered near 2142:20 as indicated by the jump in θ_e. The maximum updraft was 21 m s^{-1} near 2143:05 and located within the BWER. Large particles were observed near the northwest edge of the updraft (2143:50) but not within the main updraft. The turbulence within the main updraft was weak, suggesting an accelerating flow, and θ_e remained nearly constant across the updraft, indicative of an adiabatic core. The θ_e values at this time were slightly lower than the θ_e values observed earlier in the flight. However, this is thought to have been due to normal nocturnal cooling at the surface with a corresponding cooling and lowering of the cloud base. The horizontal extent of the main updraft at the flight altitude was approximately 5 km. The horizontal winds near the updraft maxima were from 190° at 12 m s^{-1}. The slope of the air parcel trajectories, with respect to the storm motion, was approximately 45° pointing north-northwest.

A second updraft > 10 m s^{-1} was observed within the turbulent echoing region northwest of the BWER. Vigorous secondary updrafts were repeatedly observed along the western edge of the WER where a branch of higher reflectivity extended southward, and closed echo contours were occasionally observed (Fig. 3, for example).

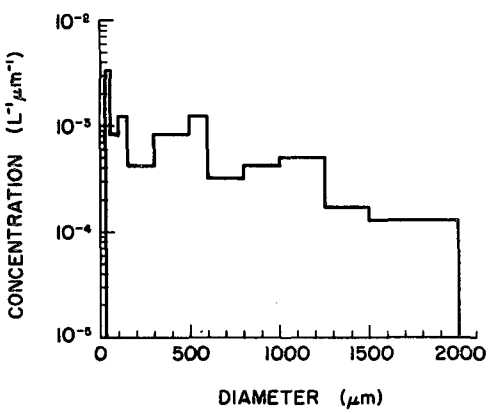

FIG. 11. Size distribution for the graupel shown in Fig. 10.

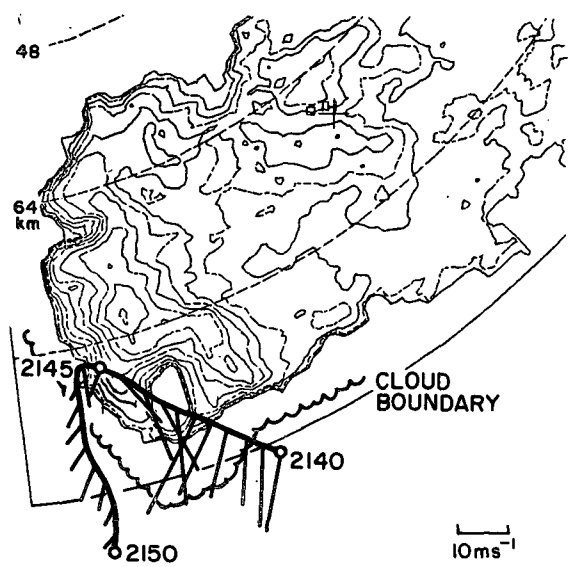

FIG. 12. As in Fig. 7, except that the PPI is at 2142 and the aircraft track is for penetration 5.

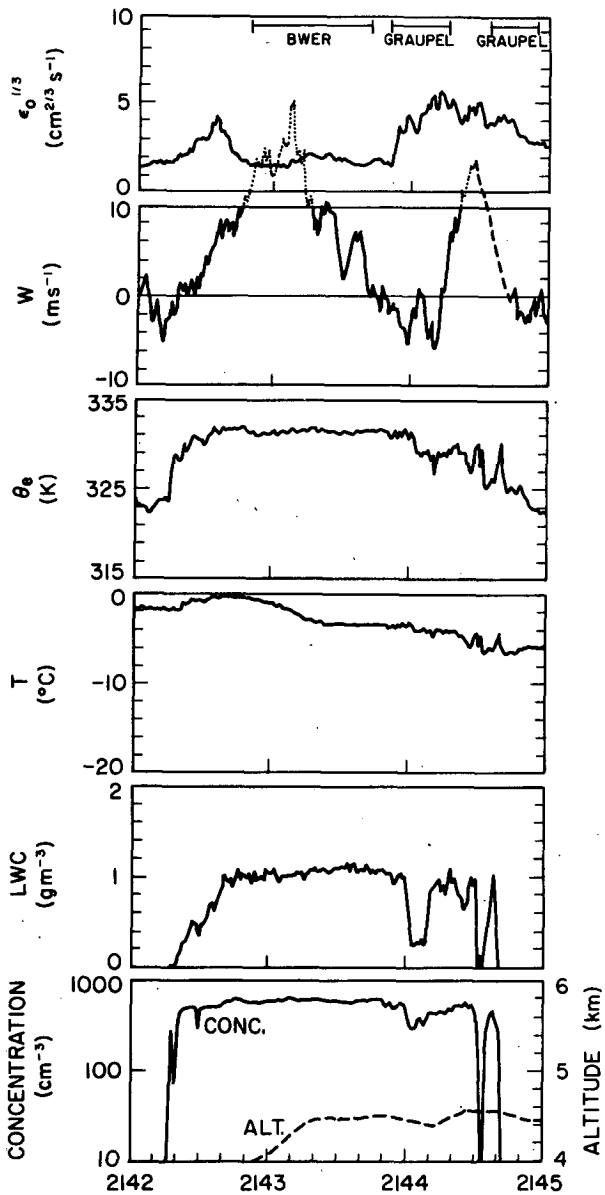

FIG. 13. As in Fig. 9, except for penetration 5.

6. Discussion

Observations of the microphysical composition and thermodynamic and kinematic structure within an Alberta supercell storm have been presented. Photographs and the aircraft measurements indicate that feeder clouds and multiple updrafts existed within the storm. The typical microphysical conditions observed within the feeder clouds in the new growth zone were consistent with theoretical calculations for similar conditions (Braham, 1968; Hindman and Johnson, 1972; Heymsfield, 1982), indicating that ice particles grow to millimeter size graupel in ~10 min. The feeder cloud lifetimes were sufficient to produce millimeter size graupel particles. The only precipitation size particles encountered by the aircraft were graupel which formed as a result of the accretional growth of ice crystals. The formation of graupel particles is of direct relevance to the problem of hail growth for the Acme storm since only graupel hailstone embryos were found. Graupel particles were observed within the base of the echo overhang. However, large particles were not found within the main updraft directly below the echo overhang. These observations suggest that the echo comprising the overhang originated and descended from higher levels and was not due to particles growing within a single ascent from cloud base.

The penetrations by N10UW were below the altitude at which Browning and Foote (1976) proposed that particles within the main updraft of supercell storms enter the overhang and travel around the southern edge of the BWER, and descend before re-entering the main updraft. Although this type of particle recirculation is one possible source of hailstone embryos, it is not supported by the storm relative winds within the WER of the Acme storm, or by the motion of cells which were tracked over and around the WER. The data synthesis from this study suggests that the likely source of the graupel embryos within the overhang was the feeder clouds within the new growth zone.

A conceptual model of the precipitation processes leading to the formation of hail within the Acme storm is presented in Fig. 14. The vertical cross section depicted in the figure is oriented parallel to the storm propagation vector **AB**. An important question regarding hail growth mechanisms (Ludlam, 1958) is: How do hail embryos remain in a region of supercooled water long enough to grow into hailstones? Graupel particles originating within the time-dependent updrafts associated with feeder clouds were in a position to be transported by the midlevel winds toward the WER where they could grow to large hail along the edge of the main storm updraft. This mechanism can account for the observed graupel and the formation and motion of the fine-scale reflectivity cells within the overhang. The great extent of the main updraft assured interaction with practically every feeder cloud that merged on the southern flank of the storm. The foregoing conceptual model is consistent with the assertion that hail embryos grow in one set of conditions and then are injected into another set of conditions more conducive to the growth of large hail (Knight and Knight, 1970). The need for this type of two-stage growth process was proposed in general terms by Marshall and Hitschfeld (1973).

The Doppler radar analysis by Heymsfield (1978) has also shown updraft substructures within an Oklahoma supercell storm. Heymsfield *et al.* (1980) concluded that the peak hail production within a Colorado multicell hailstorm resulted when graupel particles, which grew within the updraft region of a feeder cell, were transported by the wind field and fell into the main updraft region where they continued to grow. It

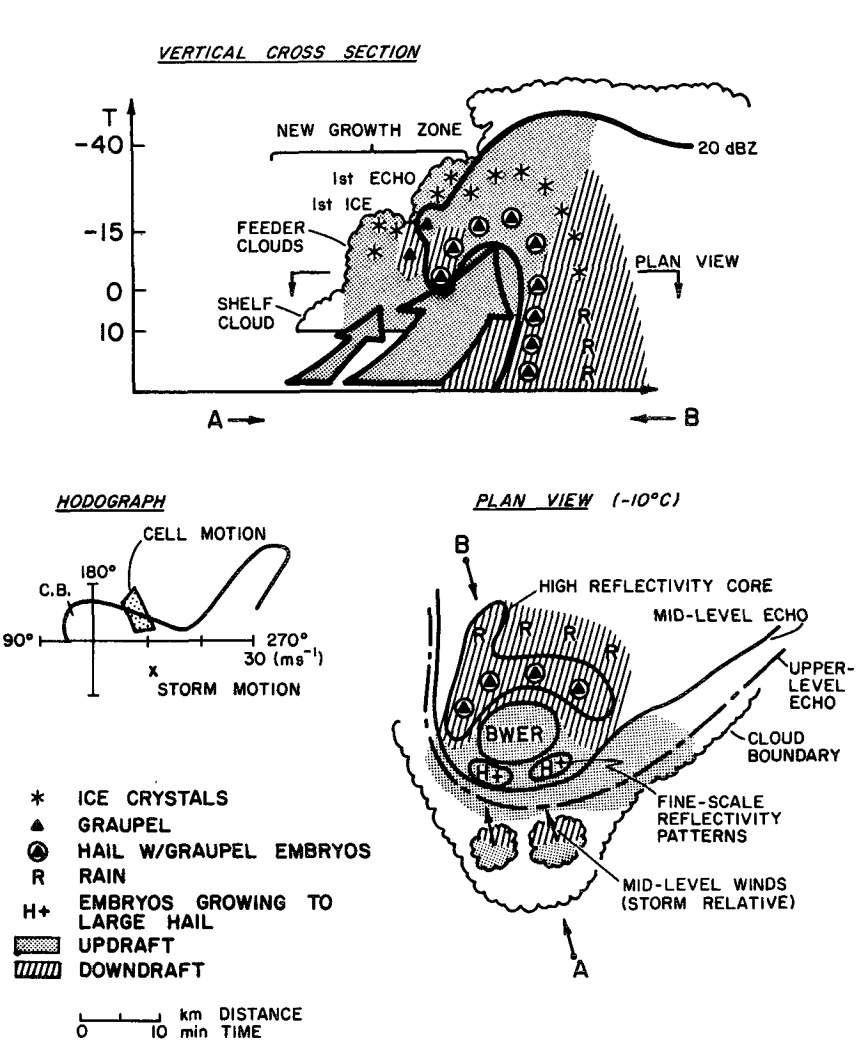

FIG. 14. A conceptual model of the precipitation processes leading to the formation of hail in the Acme storm.

is encouraging that independent studies using quite different observations of Colorado, Oklahoma and Alberta hailstorms exhibit a similar mechanism responsible for the growth of the largest hail. The evidence suggests that time-dependent, fine-scale convective cells (feeder clouds) are found within all storms and they represent a vital link among hail formation processes within a broader scale continuum of hailstorm structures.

Acknowledgments. The study reported herein is a portion of a Ph.D. thesis which T. W. Krauss completed at the University of Wyoming. The constructive criticisms of W. A. Cooper, J. C. Fankhauser, R. G. Humphries and D. L. Veal are gratefully acknowledged. We would like to express our appreciation to B. L. Barge, M. English, G. G. Goyer, J. H. Renick and the staff of the Atmospheric Sciences Department at the Alberta Research Council for their cooperation. The efforts of the pilot, G. Bershinsky, and the supporting staff at the University of Wyoming deserve special thanks. We are grateful to N. C. Knight for the hail embryo analysis. This project was funded by the Department of Agriculture of Alberta and the Alberta Research Council.

REFERENCES

Barge, B. L., and F. Bergwall, 1976: Fine scale structure of convective storms associated with hail production. Atmos. Sci. Div. Rep. 76-2, Alberta Research Council, Edmonton, 43 pp.

Braham, R. R., 1968: Meteorological basis for precipitation development. *Bull. Amer. Meteor. Soc.*, **49**, 343–353.

Browning, K. A., 1965a: The evolution of tornadic storms. *J. Atmos. Sci.*, **22**, 664–668.

——, 1965b: Some inferences about the updraft within a severe local storm. *J. Atmos. Sci.*, **22**, 669–677.

——, 1977: The structure and mechanisms of hailstorms. *Hail: A Review of Hail Science and Hail Suppression. Meteor. Monogr.*, No. 38, Amer. Meteor. Soc., 1–43.

——, and F. H. Ludlam, 1962: Airflow in convective storms. *Quart. J. Roy. Meteor. Soc.*, **88,** 117–135.

——, and R. J. Donaldson, Jr., 1963: Airflow and structure of a tornadic storm. *J. Atmos. Sci.*, **20,** 533–545.

——, and G. B. Foote, 1976: Airflow and hail growth in supercell storms and some implications for hail suppression. *Quart. J. Roy. Meteor. Soc.*, **102,** 499–533.

Byers, H. R., and R. R. Braham, Jr., 1949: *The Thunderstorm.* U.S. Govt. Printing Office, Washington, DC, 287 pp.

Chisholm, A. J., 1970: Alberta hailstorms: A radar study and model. Ph.D. thesis, McGill University, 287 pp.

Cooper, W. A., and C. P. R. Saunders, 1980: Winter storms over the San Juan Mountains. Part II: Microphysical processes. *J. Appl. Meteor.*, **19,** 927–941.

English, M., 1973: Alberta hailstorms. Part II: Growth of large hail in the storm. *Alberta Hailstorms. Meteor. Monogr.*, No. 36, Amer. Meteor. Soc., 37–98.

Foote, G. B., and J. C. Fankhauser, 1973: Airflow and moisture budget beneath a northeast Colorado hailstorm. *J. Appl. Meteor.*, **12,** 1330–1353.

Heymsfield, A. J., 1982: A comparative study of the rates of development of potential graupel and hail embryos in high plains storms. *J. Atmos. Sci.*, **39,** 2867–2897.

——, A. R. Jameson and H. W. Frank, 1980: Hail growth mechanisms in a Colorado storm. Part II: Hail formation processes. *J. Atmos. Sci.*, **37,** 1779–1807.

Heymsfield, G. M., 1978: Kinematic and dynamic aspects of the Harrah tornadic storm analyzed from dual-Doppler radar data. *Mon. Wea. Rev.*, **106,** 233–254.

Hindman, E. E., and D. B. Johnson, 1972: Numerical simulation of ice particle growth in a cloud of supercooled water droplets. *J. Atmos. Sci.*, **29,** 1313–1321.

Humphries, R. G., and B. L. Barge, 1979: Polarization and dual-wavelength radar observations of the bright band. *IEEE Trans. Geosci. Electron.*, **GE-17,** No. 4, 190–195.

Knight, C. A., and N. C. Knight, 1970: Hailstone embryos. *J. Atmos. Sci.*, **27,** 659–666.

Ludlam, F. H., 1958: The hail problem. *Nubila,* **1,** 12–96.

Marshall, J. S., and W. F. Hitschfeld, 1973: A source of hail embryos. *Atmosphere,* **11,** 195–196.

Marwitz, J. D., 1972a: The structure and motion of severe hailstorms. Part I: Supercell storms. *J. Appl. Meteor.*, **11,** 166–179.

——, 1972b: The structure and motion of severe hailstorms. Part II: Multicell storms. *J. Appl. Meteor.*, **11,** 180–188.

——, 1972c: The structure and motion of severe hailstorms. Part III: Severely sheared storms. *J. Appl. Meteor.*, **11,** 189–201.

——, and E. X. Berry, 1971: The airflow within the weak echo region of an Alberta hailstorm. *J. Appl. Meteor.*, **10,** 487–492.